Multi objective path planning for the 6-6 Stewart platform manipulator using the singularity free tube

Nishanth Adithya Chandramouli[1], Aditya Mahesh Kolte[1], Shashank Ramesh[2], and Sandipan Bandyopadhyay[1]

[1] Department of Engineering Design, Indian Institute of Technology Madras, Chennai 600036, Tamil Nadu, India,
[2] Department of Mechanical Engineering, University of Notre Dame, Notre Dame, IN 46556, USA

Abstract. A multi objective approach for constant-orientation singularity-free path planning for the 6-6 semi-regular Stewart platform manipulator (SRSPM) is presented in this paper. The concept of the *singularity-free tube* (SFT), which is described as a one-parametric family of singularity-free spheres, is utilised to ensure that the obtained paths are free of any *gain-type* singularities. *Non-Dominated Sorting Genetic Algorithm* (`NSGA-II`) is used to obtain a set of optimal paths connecting two given points while minimising its length and maximising its distance from the boundary of the SFT.

Keywords: Semi-regular Stewart platform manipulator, Path planning, Gain-type singularities, Singularity-free tube, `NSGA-II`

1 Introduction

Parallel manipulators have smaller workspaces when compared to their serial counterparts. The existence of *gain-type*[3] singularities inside the workspace restricts the workspace further. Thus, singularity-free path planning for parallel manipulators, specifically, ones with 6-degree-of-freedom (DoF), is challenging. Random exploration and probabilistic road maps (PRM) are two of many established methods employed for path planning of a 6-DoF parallel manipulator, namely, the Stewart platform manipulator (SPM). For example, in [2], the PRM method is utilised to identify safe via-points for the singularity-free path and to discretise and analyse the SPM's workspace using flood-filling algorithms. Likewise, in [3], a local routing methodology based on line geometry finds a singularity-free path once the workspace is discretised using slicing techniques. The present paper focuses on the constant orientation singularity-free path planning of an SRSPM (shown in Fig. 1a). In [4], the concept of an SFT was introduced, which is described by a one-parametric family of spheres containing a source and a destination

[3] When the end-effector of a manipulator, which in the case of parallel manipulators is usually the moving platform, acquires one or more degree-of-freedom and can move instantly or even finitely while the inputs are held fixed, it is referred to as a gain-type singularity (see, e.g., [1]) singularities. Since these occur when two or more branches of forward kinematics merge, these are also known as the *forward-kinematic* singularities.

point and is free of gain-type singularities for a constant orientation of the SRSPM. The description of the SFT in the closed-form enables the use of numerical techniques to impose additional constraints and specify various objectives related to singularity-free path planning. The SFT thus presents an infinitude of singularity-free paths between the given pair of points. In the current paper, leveraging the analytical nature of the SFT, a multi objective optimisation problem has been formulated to obtain singularity-free paths between two given points.
The rest of the paper is organised as follows: Section 2 describes the geometry of the SRSPM. Section 3 presents the steps followed in formulating and solving the optimisation problem. A numerical example and the main results are presented in Section 4. A discussion of the results obtained and conclusions are presented in Sections 5 and 6, respectively.

2 Geometry of the SRSPM

The SRSPM, a type of 6-SPS (spherical-prismatic-spherical) spatial parallel manipulator, is depicted in Fig. 1. The manipulator has six linear actuators, denoted by l_i, $i = 1, \cdots, 6$. They are coupled to the fixed platform (FP) and the moving platform (MP) via spherical joints. The symbols r_{m} and r_{f} represent the circumradii of the MP and FP, respectively. The spherical joints are centred at the vertices of both the platforms. The following represents the angular displacements of the spherical joints on the FP as measured w.r.t. the positive $\boldsymbol{X}$-axis in a counter clock wise (CCW) manner:

$$\begin{aligned}\boldsymbol{\gamma}_{\mathrm{f}} &\coloneqq [\gamma_{\mathrm{f}1}, \gamma_{\mathrm{f}2}, \gamma_{\mathrm{f}3}, \gamma_{\mathrm{f}4}, \gamma_{\mathrm{f}5}, \gamma_{\mathrm{f}6}]^{\top}, \\ &= [0, 2\gamma_{\mathrm{f}}, 2\pi/3, 2\gamma_{\mathrm{f}} + 2\pi/3, 4\pi/3, 2\gamma_{\mathrm{f}} + 4\pi/3]^{\top}. \end{aligned} \tag{1}$$

Accordingly, the coordinates of the vertices of the FP, denoted by $\boldsymbol{b}_i$, $i = 1, \cdots, 6$, in the fixed frame $\boldsymbol{O}$-$\boldsymbol{XYZ}$, are:

$$\boldsymbol{b}_i = \boldsymbol{R}_Z(\boldsymbol{\gamma}_{\mathrm{f}i})[r_{\mathrm{f}}, 0, 0]^{\top}, \tag{2}$$

where $\boldsymbol{R}_Z(\phi)$ is the *rotation matrix* describing a rotation about the positive $\boldsymbol{Z}$-axis, through an angle ϕ, in a CCW manner. Similarly, the angular displacements of the spherical joints, mounted on the MP, measured CCW from the positive $\boldsymbol{x}$-axis of the moving frame $\boldsymbol{o}$-$\boldsymbol{xyz}$, are:

$$\begin{aligned}\boldsymbol{\gamma}_{\mathrm{m}} &\coloneqq [\gamma_{\mathrm{m}1}, \gamma_{\mathrm{m}2}, \gamma_{\mathrm{m}3}, \gamma_{\mathrm{m}4}, \gamma_{\mathrm{m}5}, \gamma_{\mathrm{m}6}]^{\top}, \\ &= [0, 2\gamma_{\mathrm{m}}, 2\pi/3, 2\gamma_{\mathrm{m}} + 2\pi/3, 4\pi/3, 2\gamma_{\mathrm{m}} + 4\pi/3]^{\top}. \end{aligned} \tag{3}$$

The vertices of the MP in $\boldsymbol{o}$-$\boldsymbol{xyz}$, denoted by $\boldsymbol{t}_i$, as shown in Fig. 1b, are located at:

$$\boldsymbol{t}_i = \boldsymbol{R}_Z(\boldsymbol{\gamma}_{\mathrm{m}i})[r_{\mathrm{m}}, 0, 0]^{\top}. \tag{4}$$

The vertices $\boldsymbol{t}_i$, when transformed to the frame $\boldsymbol{O}$-$\boldsymbol{XYZ}$, are denoted by $\boldsymbol{a}_i$, where:

$$\boldsymbol{a}_i = \boldsymbol{p} + \boldsymbol{R}\boldsymbol{t}_i. \tag{5}$$

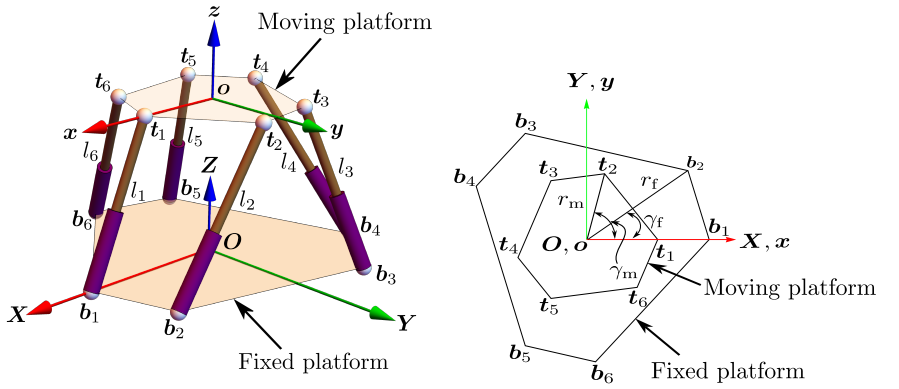

(a) Schematic of the manipulator (b) Geometry of the fixed and moving platforms

Fig. 1: Kinematic description of the SRSPM.

Table 1: Architecture parameters of an SRSPM

Parameter	**Symbol**	**Value**	**Unit**
Minimum leg length	l_{min}	0.4035	Metre
Maximum leg length	l_{max}	1.4635	Metre
Circumradii of the moving platform	r_{m}	0.6153	Metre
Circumradii of the fixed platform	r_{f}	0.9914	Metre
Half the angular spacing between the adjacent pairs of legs on the moving platform	γ_{m}	0.8656	Radian
Half the angular spacing between the adjacent pairs of legs on the fixed platform	γ_{f}	0.1256	Radian

The orientation and position of the MP with respect to $\boldsymbol{O}$-$\boldsymbol{XYZ}$ are represented by the matrix $\boldsymbol{R} \in \mathbb{S}O(3)$ and the geometric centre of the MP, $\boldsymbol{p} = [x, y, z]^\top$, respectively. The matrix $\boldsymbol{R}$ is expressed in terms of *Rodrigues parameters*, $\boldsymbol{c} = [c_1, c_2, c_3]^\top \in \mathbb{R}^3$. The architecture parameters, required to define the SRSPM, are given in Table 1.

3 Mathematical Formulation

The objective of the present work is to obtain singularity-free paths between the source and the destination points, denoted by $\boldsymbol{p}_{\text{s}} = [x_{\text{s}}, y_{\text{s}}, z_{\text{s}}]^\top$ and $\boldsymbol{p}_{\text{d}} = [x_{\text{d}}, y_{\text{d}}, z_{\text{d}}]^\top$, respectively, using multi objective optimisation.
The singularity surface, denoted by $\mathcal{S}$, for a constant orientation of the SRSPM has been derived analytically in the closed-from in [1]. The equation defining the singularity surface is reproduced below:

$$\mathcal{S} := S(x, y, z) = e_1 x^2 z + e_2 x^2 + e_3 xyz + e_4 xy + e_5 xz^2 + e_6 xz + e_7 x + e_8 y^2 z +$$

$$e_9y^2 + e_{10}yz^2 + e_{11}yz + e_{12}y + e_{13}z^3 + e_{14}z^2 + e_{15}z + e_{16} = 0. \quad (6)$$

The coefficients e_{i}, i = 1,$\cdots$,16, appearing in Eq. (6), are closed-form functions of the Rodrigues parameters c_1, c_2, c_3 and the architecture parameters r_{f}, r_{m}, $\gamma_{\mathrm{f}}, \gamma_{\mathrm{m}}$. Following [4], the projections of $\boldsymbol{p}_{\mathrm{s}}$ and $\boldsymbol{p}_{\mathrm{d}}$ onto $\mathcal{S}$ are denoted by the points, $\boldsymbol{q}_{\mathrm{s}}$ and $\boldsymbol{q}_{\mathrm{d}}$, respectively. The *geodesic curve* on $\mathcal{S}$ connecting the points $\boldsymbol{q}_{\mathrm{s}}$ and $\boldsymbol{q}_{\mathrm{d}}$, is denoted by $\mathcal{G}$. As explained in[4], the knowledge of $\mathcal{G}$ is utilised to computed the SFT (denoted by $\mathcal{T}$), in the form of a *one parameter family of spheres*:

$$\mathcal{T} \coloneqq (\boldsymbol{x} - \boldsymbol{p}_{\mathrm{c}}(t)) \cdot (\boldsymbol{x} - \boldsymbol{p}_{\mathrm{c}}(t)) - r_{\mathrm{c}}^2(t) = 0, \text{where, } \boldsymbol{x} = [x, y, z]^\top, t \in (0, 1). \quad (7)$$

The *centre curve* is given by $\boldsymbol{p}_{\mathrm{c}}(t) = [x_{\mathrm{c}}(t), y_{\mathrm{c}}(t), z_{\mathrm{c}}(t)]^\top$, while the radii of the spheres are given by the polynomial $r_{\mathrm{c}}(t)$ (see [4] for the details). A parametric polynomial path $\boldsymbol{p}_{\mathrm{p}}(t) = [x(t), y(t), z(t)]^\top$ is sought in this work, where the evolution of individual coordinates is described by distinct quintic polynomials in the path parameter $t \in [0, 1]$. The coefficients of the polynomial forming the path are estimated by formulating a constrained optimisation problem. The path is subject to the terminal constraints, namely, $\boldsymbol{p}_{\mathrm{p}}(0) = \boldsymbol{p}_{\mathrm{s}}$ and $\boldsymbol{p}_{\mathrm{p}}(1) = \boldsymbol{p}_{\mathrm{d}}$. These result in the following:

$$\begin{aligned}
x(t) &= u_{10}t^5 + u_{11}t^4 + u_{12}t^3 + u_{13}t^2 + (x_{\mathrm{d}} - u_{10} - u_{11} - u_{12} - u_{13} - x_{\mathrm{s}})t + x_{\mathrm{s}},\\
y(t) &= u_{20}t^5 + u_{21}t^4 + u_{22}t^3 + u_{23}t^2 + (y_{\mathrm{d}} - u_{20} - u_{21} - u_{22} - u_{23} - y_{\mathrm{s}})t + y_{\mathrm{s}},\\
z(t) &= u_{30}t^5 + u_{31}t^4 + u_{32}t^3 + u_{33}t^2 + (z_{\mathrm{d}} - u_{30} - u_{31} - u_{32} - u_{33} - z_{\mathrm{s}})t + z_{\mathrm{s}}.
\end{aligned}$$

The unknown coefficients are organised in the following vector:

$$\boldsymbol{\theta}_p = [u_{10}, u_{11}, u_{12}, u_{13}, u_{20}, u_{21}, u_{22}, u_{23}, u_{30}, u_{31}, u_{32}, u_{33}]^\top. \quad (8)$$

Using the knowledge of the SFT presented in [4] a dual-objective constrained optimisation problem is formulated as follows:

$$\underset{\boldsymbol{\theta}_{\mathrm{p}}}{\text{minimise}} \ \sum_{j=0}^{m} \|\boldsymbol{p}_{\mathrm{p}}(j/m) - \boldsymbol{p}_{\mathrm{c}}(j/m)\|^2, \quad (9)$$

$$\underset{\boldsymbol{\theta}_{\mathrm{p}}}{\text{minimise}} \ \int_0^1 \left(\frac{\mathrm{d}x(t)}{\mathrm{d}t}\right)^2 + \left(\frac{\mathrm{d}y(t)}{\mathrm{d}t}\right)^2 + \left(\frac{\mathrm{d}z(t)}{\mathrm{d}t}\right)^2 \mathrm{d}t, \quad (10)$$

$$\text{subject to, } \|\boldsymbol{p}_{\mathrm{p}}(j/n) - \boldsymbol{p}_{\mathrm{c}}(j/n)\|^2 - r_{\mathrm{c}}^2(j/n) < 0, \ \forall\, j \in [1, \cdots, n-1], \quad (11)$$

where, both $\boldsymbol{p}_{\mathrm{p}}(t)$ and $\boldsymbol{p}_{\mathrm{c}}(t)$ are sampled at m and n points to compute the first objective and constraint function, respectively. The two objectives, namely: (a) minimising the overall deviation of the path from the centre curve of the SFT, and (b) minimising the length of the path, are formulated in terms of Eqs. (9,10), respectively. Since the second objective is a continuous function of t, it may be computed analytically. The constraint, shown in Eq. (11), ensures that the path lies inside the SFT $\forall\, t \in [0, 1]$.

4 Illustrative example and results

For the given example, the orientation of the MP is given in terms of Rodrigues parameters, $\boldsymbol{c} = [-0.9448, 0.0703, -0.4608]^\top$, and the architecture parameters of the SRSPM

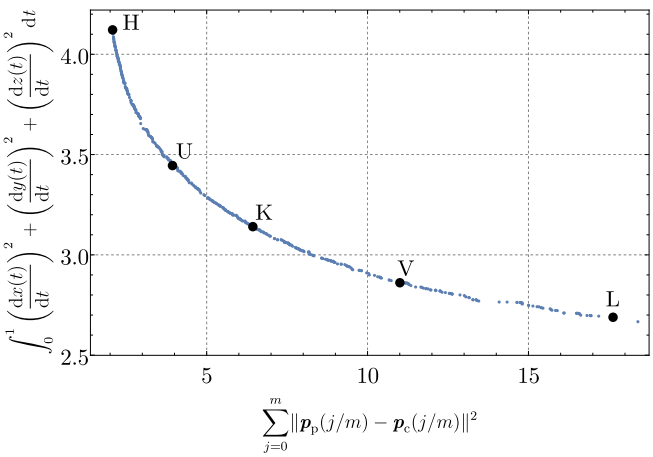

Fig. 2: Pareto front showing the solutions of the dual-objective optimisation problem.

are given in Table 1. The corresponding singularity surface $\mathcal{S}$ is computed using Eq. (6) and is shown in Fig. 3. The source point and the destination point are chosen to be, $\boldsymbol{p}_\mathrm{s} = [-0.2000, -0.5000, 0.5000]^\top$, and $\boldsymbol{p}_\mathrm{d} = [-0.0400, -0.2200, -0.3900]^\top$, respectively. These choices are arbitrary, except for two conditions: (a) both points are inside the position workspace of the manipulator corresponding to the orientation of the MP, and (b) the line segment connecting these points intersect $\mathcal{S}$; i.e., the trivial solution does not exist for the path-planning problem. Furthermore, the destination point is chosen to be fairly close to $\mathcal{S}$, so as to raise the level of difficulties in process of planning singularity-free paths. The first objective and the constraint are sampled at $m = 299$ and $n = 12$ points, respectively.

Corresponding to the numerical values mentioned above, the expressions of $x_\mathrm{c}(t)$, $y_\mathrm{c}(t)$, $z_\mathrm{c}(t)$, and $r_\mathrm{c}(t)$ are obtained as:

$$
\begin{aligned}
x_\mathrm{c}(t) &= -1.3494t^3 + 1.4785t^2 - 0.0420t - 0.0483,\\
y_\mathrm{c}(t) &= -1.2513t^3 + 1.2622t^2 + 0.0548t - 0.2648,\\
z_\mathrm{c}(t) &= -2.8460t^3 + 2.8900t^2 - 1.4962t + 0.8159,\\
r_\mathrm{c}(t) &= 20.6965t^5 - 40.2338t^4 + 22.7970t^3 - 2.6085t^2 - 1.1082t + 0.7517.
\end{aligned}
$$

Multiple solutions for $\boldsymbol{\theta}_\mathrm{p}$, corresponding to various singularity-free paths connecting $\boldsymbol{p}_\mathrm{s}$ and $\boldsymbol{p}_\mathrm{d}$, are obtained using `NSGA-II` [5]. The values for `NSGA-II` parameters are chosen based on prior experience and are presented in Table 2. A *Pareto front*[4] showing the values of the two objective functions corresponding to the obtained solutions for $\boldsymbol{\theta}_\mathrm{p}(t)$ is obtained and is shown in Fig. 2.

All the computations have been performed on a desktop computer, using one core of a Ryzen 9 7950X CPU running at 4.5 GHz. The total time taken to obtain all the so-

[4] Pareto front is a set of non-dominated solutions, being chosen as optimal, if no objective can be improved without sacrificing at least one of the other objectives.

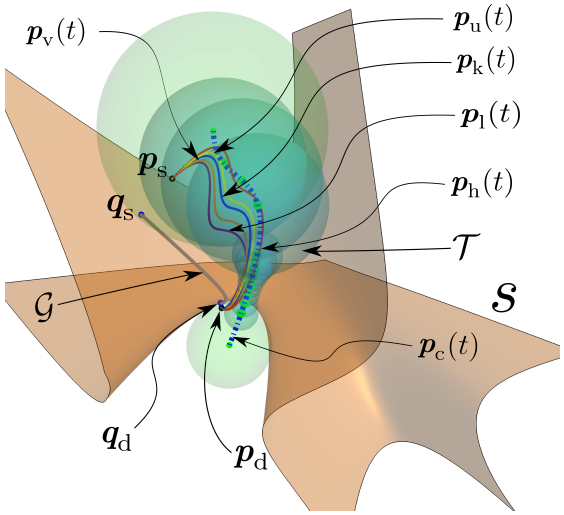

Fig. 3: Samples of singularity-free paths connecting $\boldsymbol{p}_{\mathrm{s}}$ and $\boldsymbol{p}_{\mathrm{d}}$.

lutions on the pareto front was found to be 1.658 s. From the solutions obtained, five singularity-free paths are plotted and shown in Fig. 3. The paths $\boldsymbol{p}_{\mathrm{l}}(t)$ and $\boldsymbol{p}_{\mathrm{h}}(t)$ (corresponding to the points L and H in Fig. 3) represent the *spread* of the solutions, since the others fall within these two, as expected. Figure 4 shows the residual values of Eq. (6) along the paths depicted in Fig. 3. Even though it may appear visually that the residue falls to zero (which would mean an intersection with the singularity surface) along all the paths, it is an expected consequence of the choice of the destination point close to the said surface. A look at Table 3, however, confirms that the residues do not actually vanish along any of the paths, and hence, the computed paths are indeed free of any singularity.

5 Discussions

The concept of a singularity-free tube was recently introduced in[4]. In this paper, the same has been utilised to explore the variations in singularity-free paths that can be obtained inside the SFT. Two objectives have been used in this work, which try to keep the resulting path as far as possible from the singularity surface (as approximated by the wall of the SFT) and minimise its length, respectively. All the non-dominated solutions are obtained via solution of a multi-objective optimisation problem. An entire set of singularity-free paths are obtained in less than two seconds, due to the analytical formulation of the objectives and constraint. While a polynomial model is adopted to describe the paths in this work, it is possible to any other smooth representations, such as cubic splines or NURBS. In the future, further constraints may be added to the path-planner, ensuring that the resulting path is within the workspace,

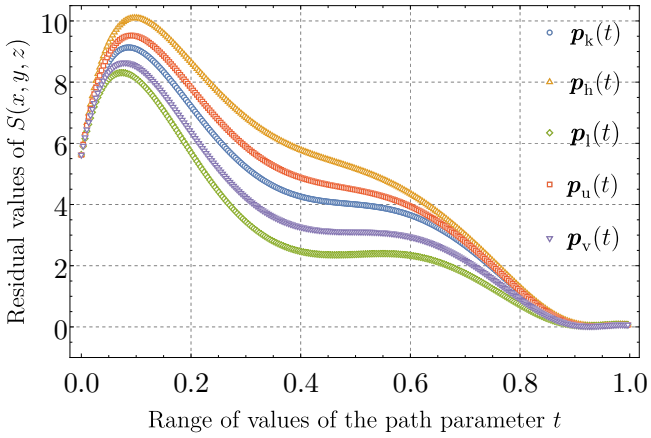

Fig. 4: A plot between the residual values of Eq. (6) and the values of the path parameter t for the paths shown in the Fig. 3.

free of link interference, and issues related to limit of motions at the passive joints.

Table 2: Chosen values of the `NSGA-II` parameters

Parameter	**Value**
Number of generations	200
Population size	500
Probability of crossover	0.9
Probability of mutation	0.167
Distribution index for crossover	100
Distribution index for mutation	20

Table 3: Minimum residual values of Eq. (6) for all the paths

Path	**Minimum residue** ($\times 10^{-2}$)
$\boldsymbol{p}_{\mathrm{k}}(t)$	2.1790
$\boldsymbol{p}_{\mathrm{h}}(t)$	3.7665
$\boldsymbol{p}_{\mathrm{l}}(t)$	2.7339
$\boldsymbol{p}_{\mathrm{u}}(t)$	2.3557
$\boldsymbol{p}_{\mathrm{v}}(t)$	2.4516

6 Conclusions

The utility of the SFT in obtaining constant orientation singularity-free paths is demonstrated by solving a multi objective constraint optimisation problem. The stated optimisation problem is solved using `NSGA-II` and the obtained solutions are presented. The multi-objective path planning method is observed to be accurate as well computationally efficient. This work serves as a step in the direction of non-singular optimal path-planning for the SRSPM which may potentially be extended to other parallel manipulators.

References

1. S. Bandyopadhyay and A. Ghosal, "Geometric characterization and parametric representation of the singularity manifold of a 6–6 Stewart platform manipulator," *Mechanism and Machine Theory*, vol. 41, no. 11, pp. 1377–1400, 2006.

2. W. Au, H. Chung, and C. Chen, "Path planning and assembly mode-changes of 6-DOF Stewart-Gough-type parallel manipulators," *Mechanism and Machine Theory*, vol. 106, pp. 30–49, 2016.
3. A. K. Dash, I.-M. Chen, S. H. Yeo, and G. Yang, "Singularity-free path planning of parallel manipulators using clustering algorithm and line geometry," in *2003 IEEE International Conference on Robotics and Automation (Cat. No. 03CH37422)*, vol. 1, pp. 761–766, 2003.
4. A. M. Kolte, S. Ramesh, and S. Bandyopadhyay, "Analytical derivation of singularity-free tubes in the constant-orientation workspace of 6-6 Stewart platform manipulators," 2024. Accepted for publication in Robotica.
5. K. Deb, A. Pratap, S. Agarwal, and T. Meyarivan, "A fast and elitist multiobjective genetic algorithm: NSGA-II," *IEEE Transactions on Evolutionary Computation*, vol. 6, no. 2, pp. 182–197, 2002.